Measurement of BOLD Changes Due to Cued Eye-Closure and Stopping During a Continuous Visuomotor Task via Model-Based and Model-Free Approaches

Govinda R. Poudel, *Member, IEEE*, Richard D. Jones, *Senior Member, IEEE*, Carrie R. H. Innes, Richard Watts, Paul R. Davidson, *Member, IEEE*, and Philip J. Bones, *Senior Member, IEEE*

***Abstract*—As a precursor for investigation of changes in neural activity underlying lapses of responsiveness, we set up a system to simultaneously record functional magnetic resonance imaging (fMRI), eye-video, EOG, and continuous visuomotor response inside an MRI scanner. The BOLD fMRI signal was acquired during a novel 2-D tracking task in which participants (10 males, 10 females) were cued to either briefly stop tracking and close their eyes (*Stop+Close*) or to briefly stop tracking *(Stop)* only. The onset and duration of eye-closure and stopping were identified *post hoc* from eye-video, EOG, and visuomotor response. fMRI data were analyzed using a general linear model (GLM) and tensorial independent component analysis (TICA). The GLM-based analysis identified predominantly increased blood oxygenation level dependent (BOLD) activity during eye-closure and stopping in multisensory areas, sensory-motor integration areas, and default-mode regions. Stopping during tracking elicited increased activity in visual processing areas, sensory-motor integration areas, and premotor areas. TICA separated the spatio-temporal pattern of activity into multiple task-related networks including the 1) occipito-medial frontal eye-movement network, 2) sensory areas, 3) left-lateralized visuomotor network, and 4) fronto-parietal visuomotor network, which were modulated differently by *Stop+Close* and *Stop*. The results demonstrate the merits of using simultaneous fMRI, behavioral, and physiological recordings to investigate the mechanisms underlying complex human behaviors in the human brain. Furthermore, knowledge of widespread modulations in brain activity due to voluntary eye-closure or stopping during a continuous visuomotor task is important for studies of the brain mechanisms underlying involuntary behaviors, such as microsleeps and attention lapses, which are often accompanied by brief eye-closure and/or response failures.**

***Index Terms*—Attention, eye-closure, functional magnetic resonance imaging (fMRI), simultaneous recording, tensorial independent component analysis, visuomotor tracking.**

I. Introduction

SIMULTANEOUS recording of continuous behavioral and physiological signals during fMRI allows investigation of the neural mechanisms underlying complex human behaviors. Most fMRI studies record impulsive responses using button presses to discretely presented stimuli, which is limiting when investigating the neural mechanisms underlying many real-life tasks in which individuals receive continuous visual and/or auditory stimuli, and for which a continuous response is required, such as driving. Recording continuous behavioral responses and associated electrophysiological signals is particularly important in the investigation of behaviors that are spontaneous in nature and require *post hoc* analysis of the data to identify the presence, onset, and duration of events.

In the current study, a system was set up to allow the simultaneous recording of eye-video, EOG, and continuous visuomotor response during fMRI scanning. The simultaneous data were recorded during an experiment aimed at investigating the neural mechanisms underlying cued eye-closure and stopping while performing a novel 2-D tracking task. The experiment was designed to simulate the real-life situation of visuomotor tracking, such as in driving, in which there can be brief intentional eye-closure and cessation of tracking to relieve physical fatigue and unintentional eye-closure due to microsleeps [1], [2]. Identifying brain activities underlying eye-closure and stopping during an active visuomotor task offers improved understanding of the neural processes underlying loss of visual input and response cessation during goal-directed visuomotor tasks. It also offers a means by which voluntary eye-closure and stopping related activity can be differentiated from the involuntary transient arousal-related activity underlying microsleeps during an active visuomotor task.

A number of studies have used fMRI to identify increased activity during voluntary eye-closure in the precentral gyrus,

Manuscript received December 13, 2009; revised February 11, 2010; accepted March 27, 2010. Date of publication June 03, 2010; date of current version October 08, 2010. This work was supported in part by Lottery Health Research, a University of Otago Postgraduate Scholarship, Foundation for Research, Science, and Technology, and Canterbury Medical Research Foundation.

G. R. Poudel and C. R. H. Innes are with the Department of Medical Physics and Bioengineering, Christchurch Hospital, 8011 Christchurch, New Zealand (e-mail: govinda.poudel@cdhb.govt.nz; carrie.innes@cdhb.govt.nz).

R. D. Jones is with the Department of Medical Physics and Bioengineering, Christchurch Hospital, Christchurch, New Zealand, Department of Medicine, University of Otago, 8011 Christchurch, New Zealand, and Department of Electrical and Computer Engineering and Department of Psychology, University of Canterbury, 8140 Christchurch, New Zealand (e-mail: richard.jones@otago.ac.nz).

R. Watts is with Department of Physics and Astronomy, University of Canterbury, 8140 Christchurch, New Zealand (e-mail: richard.watts@canterbury.ac.nz).

P. R. Davidson was with the Department of Medical Physics and Bioengineering, Christchurch Hospital, New Zealand. He is now with SLISystems Inc., 8011 Christchurch, New Zealand. (e-mail: pdavidson100@gmail.com).

P. J. Bones is with Department of Electrical and Computer Engineering, University of Canterbury, 8140 Christchurch, New Zealand (e-mail: phil.bones@canterbury.ac.nz).

Digital Object Identifier 10.1109/TNSRE.2010.2050782

1534-4320/$26.00 © 2010 IEEE

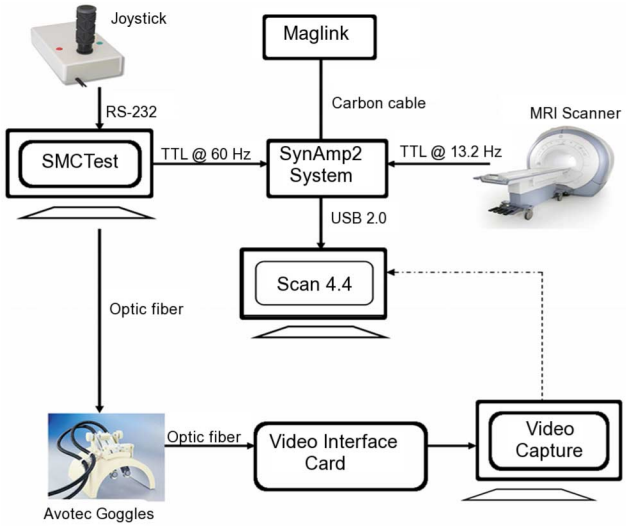

Fig. 1. Schematic of the simultaneous recording system. The SynAmp2 recording system was used to record triggers from the MRI scanner and the stimulus PC. Eye-video and EOG were synchronized by asking subjects to open and close their eyes five times immediately before and after fMRI scanning.

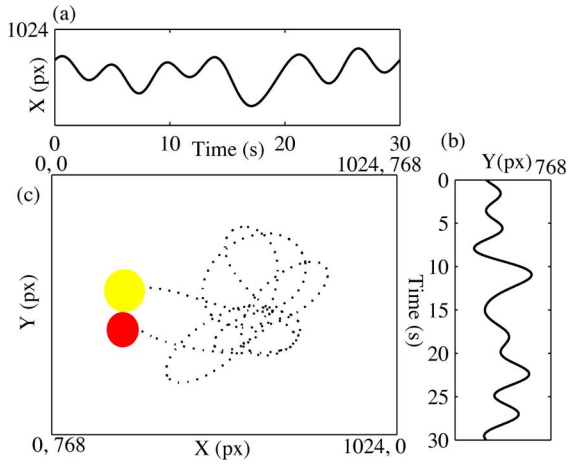

Fig. 2. The 2-D pursuit tracking task used in the study. The target path for the tracking task was defined by the sum of seven sinusoids in both horizontal and vertical direction. (a) Subjects used a joystick to follow a yellow target disc (gray) moving in a pseudorandom trajectory with a red cursor disc (black). (b) Target trajectory in x direction. (c) Target trajectory in y direction.

posterior part of the intermediate frontal gyrus (frontal eye fields), and medial superior frontal gyrus (supplementary eye field) [3]–[5]. Two of these studies have also reported increased activity in the occipital cortex, cingulate gyrus, and posterior parietal areas, with the latter also being involved in the neural mechanisms of blink suppression and visual continuity during spontaneous blinks [4], [5]. When eyes are closed for an extended time, increased activity is also observed in multiple sensory areas encompassing visual, somatosensory, vestibular, auditory, olfactory, and gustatory regions, which are believed to help maintain a so-called interoceptive state [6]–[8]. Although these studies provide important insight into neural mechanisms underlying eye-closure during rest, the neural consequences of intentional eye-closure and active suppression of visuomotor response during a visuomotor task remain unclear.

In this study, the neuronal activity, measured with fMRI, was investigated using both univariate general linear model (GLM) and multivariate tensorial independent component analysis (TICA) methods. GLM was used to identify task-related BOLD activity, whereas TICA was used to explore the dynamic interactions of brain activation regions as spatio-temporally coherent functional networks.

II. System Architecture

A system was set up to enable simultaneous recording of behavioral, electrophysiological, and fMRI data (Fig. 1). It incorporates 1) a continuous visuomotor tracking task to sample visuomotor response, 2) an MR-compatible electrophysiological data recording system, 3) an eye-video recording system, and 4) a 3T MRI scanner.

A. Visuomotor Tracking Task

A novel 2-D visuomotor tracking task was designed to sample visuomotor response with a high temporal accuracy (60 Hz). The tracking task comprises a target moving continuously (i.e., no flat spots) with a pseudo-random 2-D pattern on a computer screen. The horizontal and vertical components of the target were produced from the summation of seven sinusoids with frequencies evenly spaced from 0.033 to 0.231 Hz. The target amplitude was scaled to fit the 1024×760 pixels resolution screen. This produced a 2-D periodic target trajectory ($T = 30$ s) with a velocity range of 63–285 px/s (Fig. 2). The tracking task was presented in the MRI scanner via MR-compatible SV-7021 fibre-optic glasses (Avotec, Stuart, FL) at a resolution of 1024×768 pixels and a field-of-view of $18 \times 13°$. The target disc was 0.7° and response disc was 0.6° of visual angle in diameter.

B. EOG Recording

For EOG recording, an MR-compatible Maglink (Compumedics Neuroscan, Charlotte, NC) recording system was used. Bipolar electrodes were placed above and below the left eye to record vertical EOG. The signal was transmitted via carbon fibres (MagLink), passed through a waveguide and RF shield, and amplified using SynAmps2 amplifiers and recorded using Scan 4.4 recording system. The data were acquired at 10 kHz, after low-pass filtering with a cutoff at 2 kHz.

C. Eye-Video Recording

The Visible Eye system (Avotec Inc., Stuart, FL) incorporating a fibre-optic camera in the scanner was set up for eye-video recording. The video captured inside the MRI scanner was transmitted outside the scanner and recorded using a custom-built video recording software at 25 fps.

D. fMRI Acquisition

A Signa HDx 3.0T MRI Scanner (GE Medical Systems, Waukesha, WI) was used for structural and fMRI scanning. High resolution anatomical images of the whole brain were acquired using T1-weighted anatomical scans (repetition time (TR): 6.5 ms; echo time (TE): 2.8 ms; inversion time (TI): 400 ms; field-of-view (FOV): 225×250 mm; matrix: 512×512; slice thickness: 1 mm; number of slices: 158;

scan time: 4.5 min). Functional images were acquired using echo-planar imaging (TR: 2.5 s; TE: 35 ms; FOV: 220×220 mm; slice thickness: 4.5 mm; number of slices: 33; number of volumes: 240; scan time: 10 min). The first five images of each session were discarded to allow for T1 equilibration. A fieldmap was acquired for each subject to enable correction of EPI distortion due to magnetic field inhomogeneity (echo spacing: 700 us; TR: 580 ms; TE: 6.0 ms and 8.2 ms).

E. Synchronization

To maintain synchrony between fMRI, EOG, eye-video, and visuomotor response, the SynAmp2 recording system was used as a master clock. The MRI scanner sent a timestamp for each slice acquired and the stimulus PC sent a timestamp for each response sample (60 Hz) to the SynAmp2 system. By this means, each MRI slice and each tracking response sample was synchronized to the EOG recording system. The eye-video was synchronized with the EOG recording by asking subjects to briefly open and close their eyes five times at the start and end of the session, identifying eye-video frames and EOG samples corresponding to each eye-closures, and generating linear conversion parameter for converting each eye-video frames to EOG samples.

III. Experimental Study

A. Subjects

Twenty right-handed volunteers (10 males and 10 females, aged 21–45 years, mean 29.2 years) with no history of neurological, psychiatric, or sleep disorder participated in the study. All subjects provided informed consent according to the ethical approval from the local ethics committee.

B. Experiment

At a time between 1:00 pm and 4:00 pm, each subject took part in a 10-min session inside a MRI scanner. An MR-compatible finger-based joystick (Current Designs, Philadelphia, PA) was placed on the lower abdomen of each participant as they lay supine inside the MRI scanner. The subject held the joystick shaft with the thumb and index fingers of their right hand, which was positioned palm down. The vertical and horizontal positions of the joystick were sampled at 60 Hz and presented as a response disc.

An event-related design with an interstimulus time of 12 s was used to pseudorandomly present 3-s cues for eye-closure and stopping. Each cue was presented 24 times during the experiment. Subjects were instructed to control the joystick position so that the response disc was as close as possible to the centre of the moving target at all times except when they had to 1) briefly slowly close their eyes and simultaneously stop tracking when the screen went blank (*Stop+Close*) or 2) briefly stop tracking but keep eyes open when the response disc stopped (*Stop*). Foam support was placed below the right elbow for subject comfort and to minimize hand movement during tracking.

Subjects practised the tracking task for 1 min outside and 1 min inside the scanner to become familiarized with the tracking task and cues. Participants were provided with ear plugs to reduce the high-volume acoustic noise from the scanner. Additional pads were placed on both sides of the head to minimize head motion.

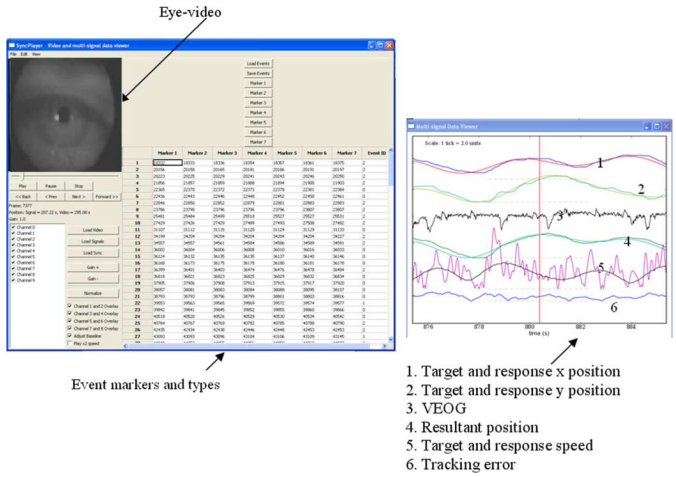

Fig. 3. The custom-built SyncPlayer program used to simultaneously replay synchronized eye-video, EOG, and tracking target (x and y), response (x and y), velocity, and error.

IV. Data Analysis

A. Data Preprocessing

The EOG data collected inside the MRI scanner was contaminated by gradient and ballistocardiogram artifacts. Gradient artifacts were effectively removed using the artifact subtraction method implemented in the Edit 4.4 software (Neuroscan, Inc.). The ballistocardiogram artifacts had a negligible effect on the large-amplitude changes in the EOG seen during eye-closure. The EOG data were then band-pass filtered at 0.5–30 Hz using a linear finite impulse response (FIR) filter and decimated to 60 Hz.

The tracking target and response signals were low-pass filtered with a cutoff at 5 Hz using a fourth-order bidirectional Butterworth filter. Resultant target and response velocities were calculated from the horizontal and vertical velocity components. Tracking error was defined as the Euclidean distance between the centres of the target and response discs.

B. Event Marking

A custom-built SyncPlayer program was used to simultaneously replay synchronized eye-video, EOG, and tracking target (x and y), response (x and y), velocity, and error (Fig. 3). An expert rater marked the onset and end of *Stop+Close* and *Stop* events by using the EOG, eye video, and tracking response signal as cues. Spontaneous blinks were also marked.

C. fMRI Preprocessing

The fMRI data were preprocessed using several modules in the FEAT (FMRI Expert Analysis Tool, Ver. 5.98) part of FSL (FMRIB's Software Library).[1] The data were realigned using MCFLIRT [9] to correct for motion due to head movement. Fieldmap-based EPI unwarping was carried out on the data using PRELUDE and FUGUE [10]. To correct for time of

[1]http://www.fmrib.ox.ac.uk/fsl

acquisition within a TR, the data were slice-time corrected using Fourier-space time-series phase-shifting. Non-brain structures were extracted from image data using BET [11]. Spatial smoothing was applied to the data using a Gaussian kernel with a 7 mm FWHM. Temporal data were high-pass filtered using Gaussian-weighted least-square straight-line fitting, with $\sigma = 75$ s. Registration to T1 anatomical images was carried out using FLIRT [9]. For group analysis, all functional scans were registered to the MNI152 standard space using the affine registration matrices derived by FLIRT and resampled to a voxel size of $3 \times 3 \times 3$ mm ^{3}. All volumes in the fMRI dataset were normalized by mean-based intensity normalization.

D. GLM Analysis of fMRI Data

The general linear model used to model the BOLD activity during *Stop*+*Close* and *Stop* was

$$h_r(t) = h_{\mathrm{Stop+Close}}(t) + h_{\mathrm{Stop}}(t) + h_{\mathrm{blinks}}(t) + h_{\mathrm{target}}(t) + m(t) + \varepsilon,$$

where $h_r\ (t)$ represents observed BOLD response, $h_{\mathrm{Stop+Close}}\ (t)$ represents BOLD activity during *Stop*+*Close*, $h_{\mathrm{Stop}}\ (t)$ represents BOLD activity during *Stop*, and $h_{\mathrm{blinks}}\ (t), h_{\mathrm{target}}\ (t)$ and $m(t)$ model spontaneous blinks, and target-related and motion-related variability in the BOLD signal. ε is the fitting error.

BOLD activity during *Stop*+*Close* was modelled using a variable epoch function, which modelled each *Stop*+*Close* trial with a boxcar epoch function of a duration equal to the duration of eye-closure in the trial, convolved with a double-gamma haemodynamic response function. The BOLD activity during *Stop* was also modelled using a regressor in the same manner as *Stop*+*Close*.

Variability due to spontaneous blinks was modelled using impulse functions set at the onset of spontaneous blinks convolved with a double-gamma haemodynamic response function. In order to take the tracking-target-related variability into account: 1) average target speed during each TR (2.5 s) was calculated using a moving-window of 2.5 s with no overlap, 2) the average target-speed time-series was scaled to a unit height, and 3) convolved with a double-gamma haemodynamic response function and used as a regressor. In order to account for any motion-related variance in the fMRI data, the effects of motion were modelled in each individual subject by the inclusion of the six motion-related parameters (estimated by the motion correction algorithm in FSL).

For each subject, the model described above was linearly fitted with the fMRI signal on a voxel-by-voxel basis using FILM [12]. Statistical contrasts were performed to identify increased or decreased activity during *Stop*+*Close* and *Stop* compared to baseline tracking, $Stop + Close > Stop$, and $Stop + Close < Stop$. The contrast maps from single-subject analysis were analyzed at the group-level $(N = 20)$ using a one-sample t-test at each voxel for each contrast of interest, using mixed-effects analysis implemented in FLAME. To correct for multiple comparisons at a group level, a cluster-based correction of the z-statistic images was performed. Statistical images were thresholded at Z-scores >2.8 to define continuous clusters. The significance level of each cluster was estimated from Gaussian Random Field theory and compared with a cluster probability threshold of 0.01 [13]. Significant clusters were then used for production of coloured blobs.

E. Tensorial Independent Component Analysis of fMRI Data

The fMRI data were also analyzed using tensorial independent component analysis (TICA) [14] as implemented in MELODIC (multivariate exploratory linear decomposition into independent components, Ver. 3.09), part of FSL. TICA decomposes data into spatial, temporal, and subject domains resulting in a tri-linear factorization of the original data such that

$$x_{ijk} = \sum_{r=1}^{R} a_{ir} b_{jr} c_{kr} + \varepsilon_{ijk}$$

in which data at voxel location j and time point i for subject k is denoted by x_{ijk}, and ε_{ijk} is the fitting error. For each estimated process r, the matrices $\mathrm{A} = [a_{ir}], \mathrm{B} = [b_{jr}]$ and $\mathrm{C} = [c_{kr}]$ represent the temporal, spatial, and subject-specific signal contributions, respectively. After voxel-wise subtraction of the mean and normalization of the voxel-wise variance, data were whitened and decomposed into a 61-dimensional subspace using probabilistic principal component analysis in which the number of dimensions was estimated using the Laplace approximation to the Bayesian evidence of the model order [15]. The whitened observations were decomposed into sets of vectors which describe signal variation across the temporal domain (time-courses), the session/subject domain, and the spatial domain (maps) by optimizing for non-Gaussian spatial source distributions using a fixed-point iteration technique [16]. Estimated component maps were divided by the standard deviation of the residual noise and thresholded by fitting a Gaussian/gamma mixture model to the distribution of voxel intensities with spatial maps and a posterior probability threshold of $p > 0.5$ [15].

Subject-mode scores obtained from TICA represent each subject's contribution to the independent components [17]. In order to identify significant independent components, a two-tailed t-test was conducted to identify components with average subject-mode scores significantly greater than 0. Therefore, only components which showed a consistent effect across the group, in that their subject scores were not driven by outliers and the mean subject score was significantly different from zero, were analyzed further. The components were then visually inspected to exclude those representing patterns with known artifacts such as head motion and high frequency noise from further analysis [15]. Multiple regression was used to identify components associated with *Stop*+*Close* and *Stop* events. Average event-related haemodynamic response functions (HRFs) for *Stop*+*Close* and *Stop* were estimated for these independent components. Task-related components with consistent event-related HRFs with a monophonic/biphasic form and peak latencies between 3 and 12 s were selected. The spatial maps of selected components were superimposed on group-averaged high-resolution T1-weighted images.

The significant statistical images obtained from both GLM and TICA analysis were superimposed on a high-resolution anatomical image. The locations of the spatial regions with

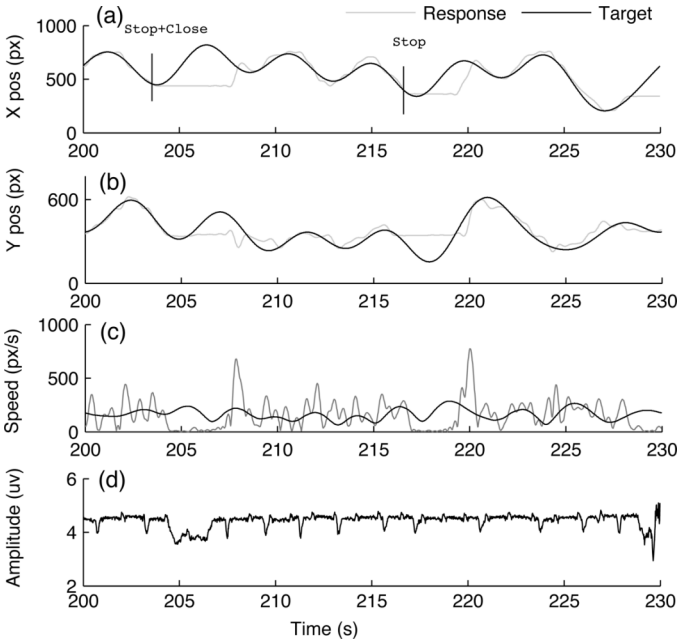

Fig. 4. Tracking behavior and EOG during Stop+Close (t = 204 s) and Stop (t = 216 s), including (a) horizontal target and response position (b) vertical target and response position, (c) target and response speed, and (d) EOG. EOG data obtained after correcting for high amplitude gradient-switching artifacts.

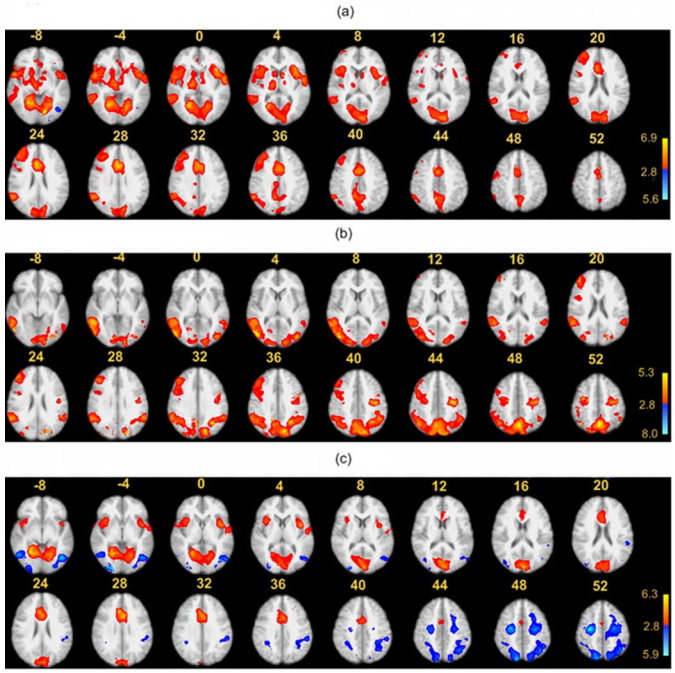

Fig. 5. Brain activation maps ($Z > 2.8, \mathrm{p} < 0.01$, corrected) for (a) Stop+Close, (b) Stop, and (c) Stop+Close versus Stop conditions obtained from GLM-based analysis of the fMRI data. The images have been registered into the standard MNI space and are shown in radiological convention.

significant BOLD activity were identified by searching for multiple local maxima in clusters and identifying their coordinates. The brain regions corresponding to the coordinates from the clusters were identified using known neuroanatomical landmarks [18] and guided by the Harvard-Oxford Cortical and Subcortical Structural Atlas (part of FSL[2]).

V. Results

A. Behavior

Each subject's eye-video, EOG, tracking response, response speed, and tracking error were used to mark the onset and end of *Stop+Close* and *Stop* events. An example of tracking response and EOG during a 10-min session is provided in Fig. 4. All subjects responded correctly to at least 90% of the *Stop+Close* trials (duration [mean $\pm$ SE] $= 1.76 \pm 0.79$ s) and *Stop* trials (duration $= 2.12 \pm 0.72$ s).

B. Brain Regions Modulated by Eye-Closure and Stopping During Tracking

The spatial map of the brain regions significantly (Z >2.8 and $p < 0.01$, corrected) modulated by *Stop+Close* during tracking obtained from GLM analysis of fMRI data is shown in Fig. 5. The brain regions showing increased and decreased activity during *Stop+Close* are presented in Table I.

As shown in the table and the spatial map, increased cortical activity was observed in the occipital cortex, middle and superior temporal cortices, posterior parietal cortex, anterior cingulate (cingulate motor area), frontal operculum, insula, and middle frontal cortex. Sub-cortical activations were also observed in the right thalamus and basal ganglia structures. Decreased activity was observed in the inferior occipital cortex.

[2]http://www.fmrib.ox.ac.uk/fsl/fslview/atlas-descriptions.html

TABLE I
Anatomical Structures, MNI Coordinates (MM), and Z-Scores Corresponding to Local Maxima of Bold Activity During *Stop+Close* (Z-Score $> 2.8, P < 0.01$, Corrected)

Brain Region	Side	Z-Score	X	Y	Z
Stop+Close > 0					
Angular Gyrus	R	4.70	52	-54	28
Middle Temporal Gyrus	R	5.37	54	-22	14
Superior Temporal Gyrus	R	4.10	56	-10	-4
Superior Temporal Gyrus	L	3.72	-58	-6	-4
Middle Frontal Gyrus	R	4.04	46	26	34
Precuneus	R	4.26	8	-52	40
Anterior Cingulate Gyrus	R	5.78	4	26	26
Supplementary Motor Cortex	R	5.15	6	-10	60
Lingual Gyrus	R	5.95	24	-58	-8
Lingual Gyrus	L	6.31	-16	-60	-16
Frontal Pole	R	4.47	12	44	-14
Insular Cortex	R	3.99	44	10	-2
Insular Cortex	L	4.10	-32	14	6
Cuneal Cortex	R	3.57	10	-88	28
Cuneal Cortex	L	4.05	-10	-84	28
Intracalcarine Cortex	R	4.12	4	-80	8
Thalamus	R	4.01	12	-14	4
Putamen	R	3.36	34	-6	-8
Occipital Fusiform Cortex	R	6.37	24	-44	-18
Occipital Fusiform Cortex	L	4.56	-28	-62	-12
Stop+Close < 0					
Inferior Lateral Occipital Cortex	L	4.57	-46	-74	-16
Occipital Pole	L	4.59	-24	-92	-18

During *Stop*, increased cortical activity (Z $>$ 2.8 and $p <$ 0.01, corrected) was observed in the occipital cortex, posterior parietal cortex, middle temporal cortex, and premotor areas (Table II).

Greater activity in the *Stop+Close* condition compared to *Stop* was found in the visual (cuneus, bilateral lingual gyri, bilateral fusiform gyri, and bilateral superior and inferior occip-

TABLE II
ANATOMICAL STRUCTURES, MNI COORDINATES (MM), AND Z-SCORES CORRESPONDING TO LOCAL MAXIMA OF BOLD ACTIVITY DURING STOP (Z-SCORE $>2.8, P < 0.01$, CORRECTED)

Brain Region	Side	Z-Score	X	Y	Z
Stop > 0					
Angular Gyrus	R	4.46	60	-52	26
Angular Gyrus	L	4.11	-50	-50	22
Cuneal Cortex	L	5.21	-16	-80	34
Inferior Temporal Gyrus	R	4.70	56	-54	-10
Intracalcarine Cortex	R	3.81	4	-84	6
Inferior Lateral Occipital Cortex	R	5.31	50	-72	2
Inferior Lateral Occipital Cortex	L	4.39	-40	-80	-6
Superior Parietal Lobule	L	3.8	-12	-66	56
Superior Lateral Occipital Cortex	R	4.56	54	-60	34
Superior Lateral Occipital Cortex	L	4.5	-18	-86	44
Lingual Gyrus	R	4.32	4	-88	-2
Middle Temporal Gyrus	R	4.66	58	-48	-4
Occipital Pole	L	4.26	-14	-94	0
Anterior Cingulate Gyrus	R	4.03	2	26	44
Precentral Gyrus	R	4.52	36	-8	52
Precentral Gyrus	L	4.62	-40	-14	50
Precuneus Cortex	M	4.59	0	-68	50
Posterior Supramarginal Gyrus	L	4.92	-54	-48	26
Supramarginal Gyrus	R	4.05	60	-46	32

ital gyri), motor (cingulate motor cortex, supplementary motor cortex), vestibular (bilateral parietoinsular cortices) and gustatory (bilateral frontal operculum) sensory areas (Table III). Decreased activity during *Stop+Close* compared to *Stop* was observed in bilateral clusters encompassing areas of the inferior lateral occipital cortex and inferior temporal gyrus, precentral gyrus, posterior parietal cortex, and superior occipital cortex.

C. Spatio-Temporally Independent Brain Networks

ITICA decomposed the multisubject fMRI dataset ($N = 20$) into 61 independent components. A subject's contribution to a specific component was represented in subject-mode score. Of the 61 components, 19 (ICs 1–13, 15, 16, 18, 21, 25, and 30) had mean subject scores significantly different from zero ($p < 0.001$, t-test, two-tailed). Six of these components (6, 7, 11, 13, 15, and 21) were removed due to an inconsistent contribution (negative subject-mode score) from multiple subjects. The 13 remaining components (1–5, 8–10, 12, 16, 18, 25, and 30) were considered for further analysis. The least-squares estimates of the 13 ICs determined that 8 components met the criteria for being related to *Stop+Close* and/or *Stop* events (Table IV). ICs 12, 16, and 18 did not show a shape of a typical HRF surrounding *Stop+Close* and/or *Stop* events and had multiple large outliers. ICs 1, 2, 3, 4, and 10 showed consistent event-related HRFs with peaks from 3 to 12 s and, hence, were considered to be task-related.

The time courses associated with IC1 (median subject score: 1.85; range: 0.72–4.2) and IC2 (median subject score: 1.80; range: 0.62–3.09) were strongly positively modulated by *Stop+Close* events (IC1: $\beta = 1.461, p < 0.001$; IC2: $\beta = 1.478, p < 0.001$). Activation clusters were found in a large area in the dorsal-medial surface of the frontal lobe corresponding to the supplementary motor cortex, right putamen, and occipital cortex. The occipital cluster encompassed parts of the superior occipital gyrus, areas of parieto-occipital sulci, and bilateral lingual gyri. Time-courses representing relative

TABLE III
ANATOMICAL STRUCTURES, MNI COORDINATES (MM), AND Z-SCORES CORRESPONDING TO LOCAL MAXIMA OF BOLD ACTIVITY DURING *STOP+CLOSE* COMPARED TO STOP (Z-SCORE $>2.8, P < 0.01$, CORRECTED)

Brain Region	Side	Z-Score	X	Y	Z
Stop+Close > 0					
Anterior Cingulate Gyrus	R	5.27	6	24	30
Anterior Cingulate Gyrus	L	5.07	-2	16	28
Cuneal Cortex	R	3.48	14	-82	28
Cuneal Cortex	L	4.59	-4	-86	24
Frontal Operculum Cortex	L	3.45	-46	16	-2
Frontal Orbital Cortex	R	3.43	36	22	16
Heschl's Gyrus	L	3.9	-56	-10	4
Insular Cortex	R	4.33	36	14	4
Insular Cortex	L	4.3	-44	6	-6
Intracalcarine Cortex	R	5.66	6	-76	8
Intracalcarine Cortex	L	5.57	-2	-76	12
Supplementary Motor Cortex	R	3.98	4	2	56
Lingual Gyrus	R	5.95	24	-58	-8
Lingual Gyrus	L	5.31	-16	-70	-12
Occipital Pole	M	5.68	0	-90	16
Temporal Occipital Fusiform Cortex	L	5.38	-22	-54	-16
Temporal Occipital Fusiform Cortex	R	5.86	24	-46	-20
Stop+Close < 0					
Inferior Lateral Occipital Cortex	R	4.6	52	-64	-8
Inferior Lateral Occipital Cortex	L	4.99	-44	-70	-10
Middle Frontal Gyrus	L	3.32	-26	10	54
Precentral Gyrus	R	5.61	30	-14	52
Precentral Gyrus	L	4.53	-20	-16	66
Supramarginal Gyrus	L	3.98	-54	-36	38
Superior Lateral Occipital Cortex	R	5.06	12	-80	48
Superior Lateral Occipital Cortex	L	4.49	-14	-72	60
Superior Parietal Lobule	R	3.51	46	-48	50
Superior Parietal Lobule	L	3.74	-44	-56	44
Inferior Lateral occipital cortex	R	4.79	26	-88	-4

TABLE IV
LEAST-SQUARES ESTIMATES OF THE MULTIPLE REGRESSIONS RELATED TO *STOP+CLOSE* AND STOP EVENTS

		Stop+Close	*Stop*	*Stop+Close - Stop*
IC1	β	1.461	-0.047	1.509
	p	(0.001)	(>0.05)	(0.001)
IC2	β	1.478	0.077	1.401
	p	(0.001)	(>0.05)	(0.001)
IC3	β	-0.915	0.027	-0.942
	p	(0.001)	(>0.05)	(0.001)
IC4	β	1.150	0.549	0.601
	p	(0.001)	(0.001)	(0.001)
IC10	β	0.500	0.089	0.411
	p	(0.001)	(>0.05)	(0.001)
IC12	β	0.692	0.293	0.398
	p	(0.001)	(0.001)	(0.001)
IC16	β	-0.540	0.036	-0.575
	p	(0.001)	(>0.05)	(0.001)
IC18	β	-0.960	-0.351	-0.609
	p	(0.001)	(0.001)	(0.001)

deactivations were observed in the bilateral insular cortex, lateral occipital cortex, paracingulate gyrus, and right postcentral gyrus. In IC2, the activation clusters were located in bilateral somatosensory regions with a large cluster in the right hemisphere covering areas of the postcentral gyrus, supramarginal gyrus, angular gyrus, and superior parietal lobule, and a smaller cluster in the left postcentral gyrus. The cluster with a local maxima in the putamen extended laterally into the frontal operculum cortex in both hemispheres. Likewise, there was a

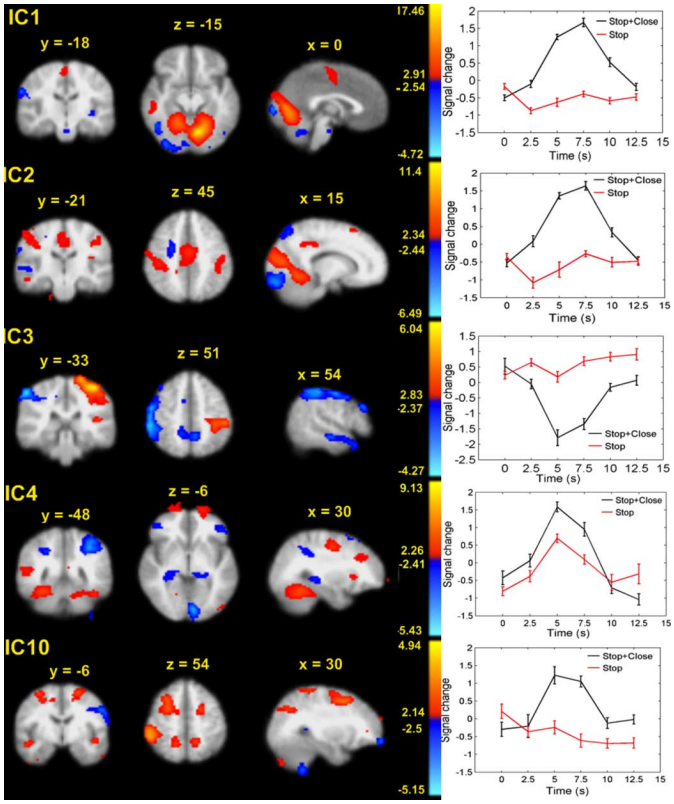

Fig. 6. The spatial map and estimated time course of the task-related ICs (1, 2, 3, 4, and 10) obtained from TICA-based analysis of the fMRI data. The vertical colour bar provides range of significant Z values associated with each IC. Images have been registered into the standard MNI space and are shown in radiological convention. The time course represents average BOLD signal change time-locked at Stop+Close and Stop events. The error bar of the time course represents the standard error of mean across all subjects.

small cluster with a local maximum in the parietal operculum cortex and extending into Heschl's gyrus.

In IC2, a large visual area in the posterior occipital lobe, bilateral frontal eye fields, ipsilateral primary motor cortex, and executive control regions including frontal pole, and anterior cingulate gyrus showed relative deactivation. Spatial maps and time courses of task-related ICs are shown in Fig. 6.

IC3 (median subject score: 1.56; range: 0.27–4.12) represented a component whose time course was negatively correlated with *Stop+Close* events ($\beta = -0.915, p < 0.001$). A smaller cluster in the premotor area of the right hemisphere and a larger cluster in the left motor areas, encompassing the postcentral gyrus and part of the superior parietal lobule, represented the areas positively correlated to the time-course of this component. Parts of the medial superior frontal gyrus in the frontal lobe were also represented by IC3. A large cluster in the right hemisphere encompassing areas of middle frontal gyrus anteriorly and angular gyrus/supramarginal gyrus posteriorly, parts of precuneus in midline, and bilateral middle/inferior temporal gyrus were negatively correlated with the time course of this component.

IC4 (median subject score: 1.80; range: 0.51–4.51) represented a component whose time course was positively correlated with both *Stop+Close* ($\beta = 1.150, p < 0.001$) and *Stop* ($\beta = 0.549, p < 0.001$) events. Activation was observed in the visual processing areas of the bilateral cuneus, bilateral insular cortices, bilateral middle temporal cortices, and a large cluster encompassing areas of the bilateral premotor, motor, and middle cingulate cortices. Relative deactivations were located in the posterior occipital lobe, superior part of the lateral occipital cortex, superior temporal gyrus, and superior parietal lobule.

The time course associated with IC10 (median subject score: 1.27; range: 0.23–3.2) was positively correlated ($\beta = 0.5, p < 0.001$) with *Stop+Close* events. The spatial pattern of this component was localized in the ventromedial frontal, middle frontal, superior parietal, superior/middle temporal, and superior occipital cortices. Relative deactivation in this component was restricted to the cingulate and inferior frontal gyri.

VI. Discussion

This is the first study to have identified the neural systems underlying cued eye-closure and stopping while performing a continuous visuomotor tracking task using BOLD fMRI signal. We were able to record EOG, eye-video, and continuous visuomotor response during fMRI scanning, which allowed us to record BOLD activities simultaneously with behaviors of interest. A novel 2-D tracking task in which the target had a minimum velocity at all points so as to have no flat-spots allowed us to sample visuomotor response with a greater and more reliable temporal accuracy. A system was developed to synchronously replay multiple behavioral data recorded inside MRI scanner so that events of interest could be identified from *post hoc* analysis of the data. The fMRI data collected in the study were analyzed using both univariate model-based and multivariate model-free approaches, which provided us with an improved understanding of the brain regions and spatiotemporally coherent cerebral networks associated with different neuronal mechanisms involved in cued eye-closure and stopping during an active task.

The behavioral context and demand associated with specific tasks employed in imaging studies need to be carefully considered [19]. In this study, simultaneous recordings of 2-D tracking performance, eye-video, VEOG, and fMRI allowed accurate identification and subsequent investigation of the events of interest. Timing of events of interest was not just based on cues but post-hoc identification from visual inspection of the simultaneous data. This is important, particularly for model-based analysis, because any slight variation in the timing of events of interest can render the effect as noise. Eye-video and VEOG allowed us to identify the onset and end of eye-closure and spontaneous blinks. Similarly, continuous recording of visuomotor responsiveness provided accurate onset and end times for stopping.

The fMRI data collected in this study were analyzed using both GLM and TICA approaches. GLM-based analysis yielded widespread patterns of increased activity in multiple cortical and sub-cortical areas during *Stop+Close* and *Stop* compared to the baseline tracking condition. While *Stop+Close* elicited increased activity in multiple sensory, oculomotor control, and default mode areas, *Stop*-related activity was concentrated in premotor and visuomotor integration areas. The *Stop+Close* related oculomotor activity observed in the current study is consistent with neuroimaging literature on eye-closure [3], [4],

[20]–[22]. Similarly, increased sensory activity during eye-closure has been attributed to maintenance of an interoceptive state [6]–[8].

Stopping elicited activities in visuomotor areas are consistently demonstrated to be active during complex finger movement tasks [23]. Likewise, activation of visual processing and parietal visuomotor areas during may be related to exertion of greater demand on these areas during abrupt stopping during visuomotor tracking [24]. These areas have been previously reported to be active during continuous visuomotor tasks such as tracking and clock drawing using joysticks [25]–[27]. The parietal visuomotor and occipital visual processing areas form a visuomotor transformation network such that lateral occipital cortex processes send visuospatial information via the posterior parietal cortex to dorsal premotor areas—all of these areas showed increased activity during stopping [21].

During *Stop+Close* and *Stop*, right-lateralized activity in the inferior/middle frontal gyrus was observed. These results are consistent with previous neuroimaging studies showing a right-lateralized response inhibition network required for suppressing an already initiated manual response [28]–[30]. They are also consistent with several event-related potential studies finding changes related to successful inhibition in right frontal regions [31], [32]. Therefore, our results suggest that inhibition of response during visuomotor tracking also operates in the right hemispheric response inhibition network.

Using TICA, we were able to separate the spatio-temporal pattern of BOLD activity into multiple task-related networks including 1) occipito-medial frontal eye-movement network (IC1, IC10), 2) sensory areas (IC2), 3) left lateralized visuomotor network (IC3), and 4) fronto-parietal visuomotor network (IC4).

IC1 represented the eye-movement-related network comprising the occipital and medial frontal cortices. Likewise, IC10 represented a network comprising the frontal eye-fields, parietal eye-fields, and posterior parietal cortex. These networks have been consistently found to be involved in different types of eye-movements including blinks and saccades [3], [4], [20]. Previous studies, along with differentiation by TICA of a close association of this network to *Stop+Close*, suggests that this brain network is particularly related to eye-movement activity. We suggest that a transient increase in activity in this network occurs when closing the eyes irrespective of baseline state and is crucial in the process of eye-lid closure during visuomotor tracking.

IC2 represents a transient increase in activity during *Stop+Close* in multiple sensory areas, including visual, somatosensory, vestibular, and auditory, which were also found to be active from GLM-based analysis. Previous research has found these areas to be active during prolonged eye-closure [6]–[8].

IC3 represents deactivation of a left lateralized fronto-parietal network, which was also found to show decreased activity during *Stop+Close* by the GLM-based analysis. This network comprises the extrastriate visual, posterior parietal, pre-motor, and middle/superior frontal cortices. Likewise, IC4 represents a activation network common for both *Stop+Close* and *Stop*. The brain regions represented in IC4 were mainly the occipital and fronto-parietal visuomotor regions.

It is important to note that most of brain regions in the networks identified by TICA were also observed in GLM analysis. However, some of the areas, such as those represented in IC10, were not observed in GLM-based analysis. This may be due to the statistical threshold used in GLM-based analysis. Since the GLM-based method used a specific model (variable-epoch model for both *Stop+Close* and *Stop*) to identify brain regions underlying *Stop+Close* and *Stop*, mismatch between the model and the nature of the BOLD response in these areas may also have resulted in the suppression of the activation pattern. Previous studies have found TICA to be more effective in isolating activity that is weaker but persistent across subjects, leading to greater and larger activation patterns than GLM-based analysis [33], [34].

The utility of TICA in the current study is two-fold. First, it provides further support to the results obtained from the more traditional GLM-based analysis. Second, it points to the usefulness of model-free schemes for separation of brain-networks involved in different brain mechanisms during the same task. This notwithstanding, TICA has a limitation in that the method often results in a large number of components, making it difficult to select components of interest and, hence, potentially introducing a bias towards some components over others if stringent criteria are not followed.

The brain networks found to be associated with Stop+Close and Stop provide an important insight into the neuronal activity underlying voluntary cessation of responsiveness during a continuous visuomotor task. Since we were interested specifically in the voluntary behaviors in this study, the task was made of short duration so as to not contaminate the data with unintentional lapses of responsiveness. Future studies should compare the brain mechanisms associated with voluntary and involuntary lapses of responsiveness by conducting an experiment with an extended version of the continuous tracking task.

In summary, we have developed a system to record simultaneous fMRI, EOG, eye-video, and continuous visuomotor response inside MRI scanner. An experiment conducted inside a MRI scanner revealed the spatial characteristics of the transient neural processes underlying cued eye-closure and stopping during a pursuit tracking task. These transient processes span widespread cortical and subcortical brain regions, mainly involved in oculomotor control, visuomotor control, and executive functions. Knowledge of widespread modulations in brain activity due to eye-closure or stopping during a continuous visuomotor task is important for studies of brain mechanisms underlying involuntary behaviors with potentially dire consequences such as microsleeps and attention lapses, which are often accompanied by brief eye-closure and/or response failures.

REFERENCES

[1] M. T. R. Peiris, R. D. Jones, P. R. Davidson, G. J. Carroll, and P. J. Bones, "Frequent lapses of responsiveness during an extended visuomotor tracking task in non-sleep-deprived subjects," *J. Sleep Res.*, vol. 15, pp. 291–300, 2006.

[2] L. N. Boyle, J. Tippin, A. Paul, and M. Rizzo, "Driver performance in the moments surrounding a microsleep," *Transportation Res. Part F: Traffic Psychol. Behav.*, vol. 11, pp. 126–136, 2008.

[3] J. Y. Chung, H. W. Yoon, M. S. Song, and H. W. Park, "Event related fMRI studies of voluntary and inhibited eye blinking using a time marker of EOG," *Neurosci. Lett.*, vol. 395, pp. 196–200, 2006.

[4] M. Kato and S. Miyauchi, "Functional MRI of brain activation evoked by intentional eye blinking," *NeuroImage*, vol. 18, pp. 749–759, 2003.
[5] D. Bristow, C. Frith, and G. Rees, "Two distinct neural effects of blinking on human visual processing," *NeuroImage*, vol. 27, pp. 136–145, 2005.
[6] E. Marx, T. Stephan, A. Nolte, A. Deutschlander, K. C. Seelos, M. Dieterich, and T. Brandt, "Eye closure in darkness animates sensory systems," *NeuroImage*, vol. 19, pp. 924–934, 2003.
[7] E. Marx, A. Deutschländer, T. Stephan, M. Dieterich, M. Wiesmann, and T. Brandt, "Eyes open and eyes closed as rest conditions: Impact on brain activation patterns," *NeuroImage*, vol. 21, pp. 1818–1824, 2004.
[8] M. Wiesmann, R. Kopietz, J. Albrecht, J. Linn, U. Reime, E. Kara, O. Pollatos, V. Sakar, A. Anzinger, and G. Fesl, "Eye closure in darkness animates olfactory and gustatory cortical areas," *NeuroImage*, vol. 32, pp. 293–300, 2006.
[9] M. Jenkinson, P. Bannister, M. Brady, and S. Smith, "Improved optimization for the robust and accurate linear registration and motion correction of brain images," *NeuroImage*, vol. 17, pp. 825–841, 2002.
[10] M. Jenkinson, "A fast, automated, n-dimensional phase unwrapping algorithm," *Magn. Reson. Med.*, vol. 49, pp. 193–197, 2003.
[11] S. M. Smith, "Fast robust automated brain extraction," *Hum. Brain Mapp.*, vol. 17, pp. 143–155, 2002.
[12] M. W. Woolrich, B. D. Ripley, M. Brady, and S. M. Smith, "Temporal autocorrelation in univariate linear modeling of FMRI data," *NeuroImage*, vol. 14, pp. 1370–1386, 2001.
[13] K. J. Friston, J. Ashburner, C. D. Frith, J. B. Poline, J. D. Heather, and R. S. J. Frackowiak, "Spatial registration and normalisation of images," *Hum. Brain Mapp.*, vol. 2, pp. 165–189, 1995.
[14] C. F. Beckmann and S. M. Smith, "Tensorial extensions of independent component analysis for multisubject FMRI analysis," *NeuroImage*, vol. 25, pp. 294–311, 2005.
[15] C. F. Beckmann and S. M. Smith, "Probabilistic independent component analysis for functional magnetic resonance imaging," *IEEE Trans. Med. Imag.*, vol. 23, no. 2, pp. 137–152, Feb. 2004.
[16] A. Hyvarinen, "Fast and robust fixed-point algorithms for independent component analysis," *IEEE Trans. Neural Networks*, vol. 10, no. 3, pp. 626–634, May 1999.
[17] Z. T. Kincses, H. Johansen-Berg, V. Tomassini, R. Bosnell, P. M. Matthews, and C. F. Beckmann, "Model-free characterization of brain functional networks for motor sequence learning using fMRI," *NeuroImage*, vol. 39, pp. 1950–1958, 2008.
[18] J. K. Mai, J. Assheuer, and G. Paxinos, *Atlas of the Human Brain*, 2nd ed. San Diego, CA: Elsevier, 2004.
[19] E. Duff, J. Xiong, B. Wang, R. Cunnington, P. Fox, and G. Egan, "Complex spatio-temporal dynamics of fMRI BOLD: A study of motor learning," *NeuroImage*, vol. 34, pp. 156–168, 2007.
[20] I. Bodis-Wollner, "Functional MRI mapping of occipital and frontal cortical activity during voluntary and imagined saccades," *Neurology*, vol. 49, pp. 416–420, 1997.
[21] H. J. Spiers and E. A. Maguire, "Neural substrates of driving behaviour," *NeuroImage*, vol. 36, pp. 245–255, 2007.
[22] T. Hanakawa, M. A. Dimyan, and M. Hallett, "The representation of blinking movement in cingulate motor areas: A functional magnetic resonance imaging study," *Cereb. Cortex*, vol. 18, pp. 930–937, 2008.
[23] K. M. Stephan, F. Binkofski, U. Halsband, C. Dohle, G. Wunderlich, A. Schnitzler, P. Tass, S. Posse, H. Herzog, and V. Sturm, "The role of ventral medial wall motor areas in bimanual co-ordination: A combined lesion and activation study," *Brain*, vol. 122, pp. 351–368, 1999.
[24] S. Gobel, V. Walsh, and M. F. S. Rushworth, "The mental number line and the human angular gyrus," *NeuroImage*, vol. 14, pp. 1278–1289, 2001.
[25] T. Ino, T. Asada, J. Ito, T. Kimura, and H. Fukuyama, "Parieto-frontal networks for clock drawing revealed with fMRI," *Neurosci. Res.*, vol. 45, pp. 71–77, 2003.
[26] J. M. Ellermann, J. D. Siegal, J. P. Strupp, T. J. Ebner, and K. Ugurbil, "Activation of visuomotor systems during visually guided movements: A functional MRI study," *J. Magn. Reson. Imag.*, vol. 131, pp. 272–285, 1998.
[27] N. Nishitani, K. Uutela, H. Shibasaki, and R. Hari, "Cortical visuomotor integration during eye pursuit and eye-finger pursuit," *J. Neurosci.*, vol. 19, pp. 2647–2657, 1999.
[28] H. Garavan, T. J. Ross, and E. A. Stein, "Right hemispheric dominance of inhibitory control: An event-related functional MRI study," *Proc. Nat. Acad. Sci. USA*, vol. 96, pp. 8301–8306, 1999.
[29] A. R. Aron, T. W. Robbins, and R. A. Poldrack, "Inhibition and the right inferior frontal cortex," *Trends in Cognitive Sci.*, vol. 8, pp. 170–177, 2004.
[30] A. R. Aron and R. A. Poldrack, "Cortical and subcortical contributions to stop signal response inhibition: Role of the subthalamic nucleus," *J. Neurosci.*, vol. 26, pp. 2424–2433, 2006.
[31] S. R. Pliszka, M. Liotti, and M. G. Woldorff, "Inhibitory control in children with attention-deficit/hyperactivity disorder: Event-related potentials identify the processing component and timing of an impaired right-frontal response-inhibition mechanism," *Biol. Psychiatry*, vol. 48, pp. 238–246, 2000.
[32] M. Schmajuk, M. Liotti, L. Busse, and M. G. Woldorff, "Electrophysiological activity underlying inhibitory control processes in normal adults," *Neuropsychologia*, vol. 44, pp. 384–395, 2006.
[33] C. F. Beckmann, M. Jenkinson, M. W. Woolrich, T. E. J. Behrens, D. E. Flitney, J. T. Devlin, and S. M. Smith, "Applying FSL to the FIAC data: Model-based and model-free analysis of voice and sentence repetition priming," *Human Brain Mapp.*, vol. 27, pp. 380–391, 2006.
[34] C. Habas and E. A. Cabanis, "Dissociation of the neural networks recruited during a haptic object-recognition task: Complementary results with a tensorial independent component analysis," *Am. J. Neuroradiol.*, vol. 29, pp. 1715–1721, 2008.

Govinda R. Poudel (S'04–M'10) received the B.E. (Hons.) degree in computer systems engineering from the University of Technology, Sydney, Australia, in 2005, and the Ph.D. degree in medicine from the University of Otago, Christchurch, New Zealand, in 2010.

He is a neuroscientist in the Department of Medical Physics and Bioengineering of Canterbury District Health Board, Christchurch, New Zealand. His research interests include the application of signal processing and statistical analysis techniques to fMRI and EEG data.

Richard D. Jones (M'87–SM'90) received the B.E.(Hons.) and M.E. degrees in electrical and electronic engineering from the University of Canterbury, Christchurch, New Zealand, in 1974 and 1975 respectively, and the Ph.D. degree in medicine from the University of Otago, Christchurch, New Zealand, in 1987.

He is Director of the Christchurch Neurotechnology Research Programme based in the Van der Veer Institute for Parkinson's and Brain Research, a Senior Biomedical Engineer and Neuroscientist in the Department of Medical Physics and Bioengineering of Canterbury District Health Board, an Adjunct Associate Professor in the Departments of Electrical and Computer Engineering, Communication Disorders, and Psychology at the University of Canterbury, and an Honorary Research Associate Professor in the Department of Medicine at the University of Otago, Christchurch. His research interests and contributions fall largely within neural engineering and the neurosciences, and particularly within 1) human performance engineering—development and application of computerized tests for quantification of upper-limb sensory-motor and cognitive function, particularly in brain disorders (stroke, Parkinson's disease, traumatic brain injury) and driver assessment, 2) lapses of responsiveness (microsleeps, attention lapses)—characteristics, brain mechanisms via simultaneous-fMRI+EEG+Tracking+EyeClosure, and detection from behavioral measures (tracking and videometrics) and electrophysiological signals (EEG, EOG), 3) signal processing in clinical neurophysiology—detection of epileptic activity, 4) eye movements in brain disorders, 5) computational modelling of the human brain, 6) virtual-reality approaches to neurorehabilitation, and 7) neural control of swallowing. He is a member of the Editorial Board of *Journal of Neural Engineering*.

Dr. Jones is a Fellow of the Institution of Professional Engineers New Zealand, a Fellow and a Past President of the Australasian College of Physical Scientists and Engineers in Medicine, a Fellow of American Institution for Medical and Biological Engineering, and a Fellow of the Institute of Physics (U.K.). He has been a member of most of the IEEE Engineering in Medicine and Biology Society's International Conference Committees since 1988, a past member of its Administrative Committee (representative for Asia-Pacific region), and Co-Chair of the Neural and Rehabilitation Engineering Theme at EMBS conferences in 2001, 2005, 2008, and 2010. He is an Associate Editor of IEEE TRANSACTIONS ON NEURAL SYSTEMS AND REHABILITATION ENGINEERING, a Theme Editor on the EMBS Conference Editorial Board, and a past Associate Editor of IEEE TRANSACTIONS ON BIOMEDICAL ENGINEERING.

Carrie R. H. Innes received B.Sc. and M.Sc. (with distinction) degrees in neuroscience from the University of Otago, Dunedin, New Zealand, in 1996 and 1999, respectively, and the Ph.D. degree in medicine from the University of Otago, Christchurch, New Zealand, in 2006.

Since 2006, she has been a Research Fellow in the Christchurch Neurotechnology Research Programme based at the Van der Veer Institute for Parkinson's and Brain Research and a Neuroscientist in the Department of Medical Physics and Bioengineering, Canterbury District Health Board, Christchurch, New Zealand. Her research is focused on "driving and accident prevention: across 1) assessment of driving-related cognitive and physical functions in persons with brain disorders and 2) behavioral and fMRI detection and characterization of involuntary microsleeps.

Richard Watts received the B.Sc. and D.Phil. degrees in physics from the University of York, York, U.K., in 1991 and 1995, respectively.

He is currently a Senior Lecturer in the Department of Physics and Astronomy at the University of Canterbury, and Director of Magnetic Resonance Research at the Van der Veer Institute for Parkinson's and Brain Research, both in Christchurch, New Zealand. He has previous held both postdoctoral and faculty positions at the Weill-Cornell Medical College, New York, and postdoctoral positions at the University of Sheffield, U.K., and the Centre d'Études Nucléaires, Grenoble, France.

Dr. Watts is a member of the International Society for Magnetic Resonance in Medicine and the Institute of Physic.

Paul R. Davidson (S'95–M'01) was born in New Zealand, in 1977. He received the B.E. (Hons.) and Ph.D. degrees in electrical and electronic engineering from the University of Canterbury, Christchurch, New Zealand, in 1998 and 2001, respectively.

He is a Senior Software Engineer at SLI Systems Inc., in Christchurch, New Zealand, where his research responsibilities include automated near-real-time data mining and statistical analysis across massive data sets. From 2005 to 2007 he was Deputy Director of the Christchurch Neurotechnology Research Programme, based at the Van der Veer Institute for Parkinson's and Brain Research in Christchurch, New Zealand. He was also a biomedical engineer and neuroscientist in the Department of Medical Physics and Bioengineering of the Canterbury District Health Board and an Adjunct Fellow in the Department of Electrical and Computer Engineering at the University of Canterbury.

Dr. Davidson was a Brain Physiology and Modeling Track Co-Chair for in EMBC 2005 Shanghai.

Philip J. Bones (M'81–SM'94) was born in Palmerston North, New Zealand, in 1951. He received the B.E. (Hons.), M.E. and Ph.D. degrees from the University of Canterbury, Christchurch, New Zealand, in 1973, 1975, and 1981, respectively.

He worked for a total of 11 years as biomedical engineer in the Department of Cardiology, Christchurch, and a further two years as postdoctoral fellow with cardiac groups in Europe (including one year as Alexander von Humboldt fellow in Heidelberg, Germany). Since 1988 he has been in the Department of Electrical and Computer Engineering, University of Canterbury, Christchurch, New Zealand. His research interests include medical imaging, problems in image recovery, and the application of signal processing techniques to physiological signals.

Prof. Bones is a member of the SPIE and ACPSEM (Australasian College of Physical Scientists and Engineers in Medicine).